ARTICLE OPEN

Check for updates

# Interaction-free, single-pixel quantum imaging with undetected photons

Yiquan Yang[1], Hong Liang[1], Xiaze Xu[1], Lijian Zhang[1], Shining Zhu[1] and Xiao-song Ma[1,2,3]✉

A typical imaging scenario requires three basic ingredients: (1) a light source that emits light, which in turn interacts and scatters off the object of interest; (2) detection of the light being scattered from the object and (3) a detector with spatial resolution. These indispensable ingredients in typical imaging scenarios may limit their applicability in the imaging of biological or other sensitive specimens due to unavailable photon-starved detection capabilities and inevitable damage induced by interaction. Here, we propose and experimentally realize a quantum imaging protocol that alleviates all three requirements. By embedding a single-photon Michelson interferometer into a nonlinear interferometer based on induced coherence and harnessing single-pixel imaging technique, we demonstrate interaction-free, single-pixel quantum imaging of a structured object with undetected photons. Thereby, we push the capability of quantum imaging to the extreme point in which no interaction is required between object and photons and the detection requirement is greatly reduced. Our work paves the path for applications in characterizing delicate samples with single-pixel imaging at silicon-detectable wavelengths.

*npj Quantum Information* (2023)9:2 ; https://doi.org/10.1038/s41534-022-00673-6

## INTRODUCTION

Over the past few decades, several imaging protocols based on quantum technologies have been realized[1,2], which have expanded the application capabilities of optical imaging. These include ghost imaging (GI)[3,4], quantum imaging with undetected photons (QIUP)[5], and interaction-free measurements (IFMs)[6,7]. The quantum GI scheme relies on the spatial correlations of entangled photon pairs and requires two-photon coincident measurements. Furthermore, ghost imaging can also be realized with classical intensity-fluctuation correlations[8]. Later, various single-pixel imaging (SPI) protocols were proposed[9–13], where the spatial correlations are not between two photons but between one photon and a programmable mask held in a spatial light modulator (SLM).

In contrast to modern digital cameras employing array sensors to capture images, SPI use a sequence of masks to interrogate the scene along with the correlated intensity measurements by a single-pixel detector. The spatially resolved masks are usually generated by computer and displayed by SLM. Combined with compressive techniques[10], the number of sampling measurements is fewer than the total number of pixels in the image. Thereby, SPI can reduce the data processing requirement, and shows potential capability for high dimensional sensing[12]. On the other hand, the modern single-photon detector is featured by improved detection efficiency, lower dark counts, and faster timing response[14]. Such enhancements have significance to applying SPI into weak signal detection scenarios, such as scattering medium imaging or long-range 3D imaging[11].

The QIUP scheme is based on induced coherence (IC), which was first proposed by Zou, Wang, and Mandel[15]. They used two photon sources to generate photon pairs. By overlapping path of two sources for one photon (idler)[15–17] and establishing the so-called path identity[18,19], there is no information about the origin of the other photon (signal). Thus, the signal photon is in the superposition state of being created in either of the sources. The phase and transmissivity of the idler photon are encoded in the interference of the signal photon. Inserting one object onto the idler path between two sources, one can obtain images exclusively with the signal photons which have no interaction with the object[5]. In contrast to GI, QIUP does not involve the detection of the photon illuminating the object or any coincidence measurement. This is an advantage of QIUP, as the wavelength of the detected photon can be chosen independently from that of the photon interacting with the object[5]. This concept was further explored in infrared (IR) spectroscopy[20], optical coherence tomography[21,22], mid-IR imaging[23–25], terahertz (THz) sensing[26], biological microscopy[27], and holography[28]. Recently, the related SU(1,1) interferometer has been investigated and employed in quantum-enhanced metrology[29–33].

However, both GI and QIUP require direct interaction between the object and the probe photon. By contrast, IFM allows one to detect the presence of a photon-supersensitive object without direct interaction. Dicke coined the name 'IFM'[6]. Elitzur and Vaidman (EV) proposed the concrete method to realize IFM[7]. In the EV scheme, the Mach-Zehnder interferometer (MZI) is aligned to have destructive interference at the dark output in the absence of the object. As one opaque object was placed onto either path of the interferometer, the presence of the object modifies the optical interferograms of the MZI. Any photon detection event at the dark port indicates the photon comes from the path not containing the object. Hence, the measurements for binary objects were deemed interaction-free. For grey or quantum objects, Kwiat et al. considered 'quantum interrogation' as a more appropriate terminology[34]. High-efficiency IFMs have also been realized by using the discrete quantum Zeno effect[34–36]. Later, exploiting the advantages of the lithographically written waveguides, highly efficient IFMs with an integrated chip have been

[1]National Laboratory of Solid-State Microstructures, School of Physics and Collaborative Innovation Center of Advanced Microstructures, Nanjing University, Nanjing 210093, China. [2]Synergetic Innovation Center of Quantum Information and Quantum Physics, University of Science and Technology of China, Hefei 230026, China. [3]Hefei National Laboratory, Hefei 230088, China. ✉email: xiaosong.ma@nju.edu.cn

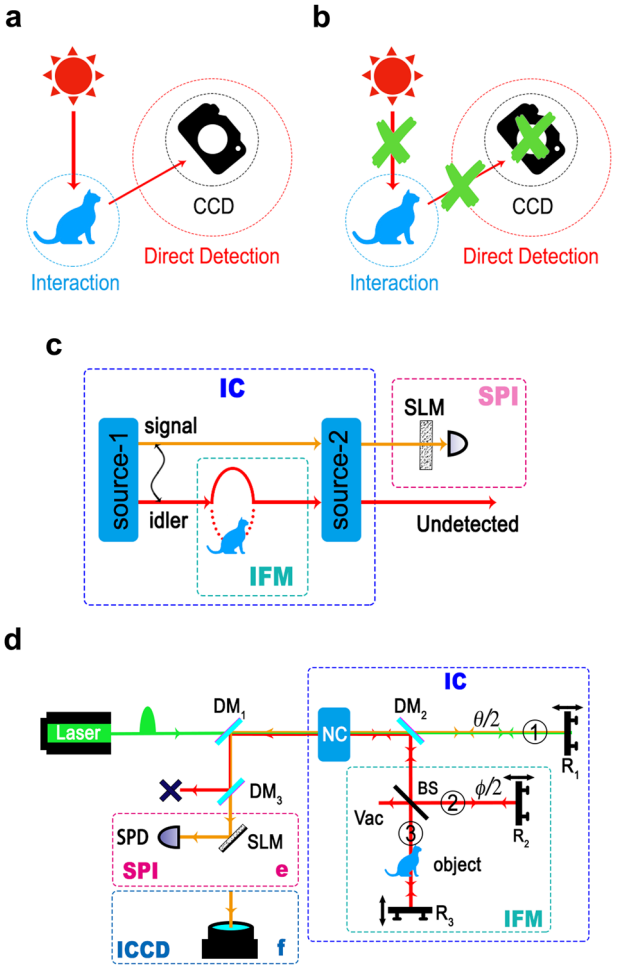


**Fig. 1 Conceptual scheme and setup of interaction-free, single-pixel quantum imaging with undetected photons. a** Classical imaging. Classical imaging requires a light source that emits light, which in turn interacts with the object of interest; a detector with spatial resolution directly detects light scattered from the object. **b** In our imaging scheme, all the above conditions are alleviated, which means imaging can be realized without direct interaction, direct detection, and a charge-coupled device (CCD) camera. **c** Conceptual diagram. Our imaging protocol is realized by integrating two interferometers based on the induced coherence (IC) and the interaction-free measurement (IFM) with the single-pixel imaging (SPI). **d** Experimental setup. A folded version of panel (**c**) realizes IC. The double-pass spontaneous parametric down-conversion processes correspond to source-1 and source-2 in panel (**c**). The IFM is realized with a single-photon Michelson interferometer. The object is placed into arm ③ of the IFM. Vac denotes the vacuum port of the IFM module. The idler photon is filtered out by dichroic mirror $DM_3$ and remains undetected throughout the entire imaging process. The circled numbers represent different arms of the interferometer. $\theta$ and $\phi$ represent the phase of the signal photon and the relative phase of the IFM. We also perform interaction-free quantum imaging with an intensified CCD (ICCD) camera (shown in inset **f** of panel d), instead of using SPI (shown in inset **e** of panel d). IC induced coherence, IFM interaction-free measurement, SPI single-pixel imaging, SLM spatial light modulator, DM dichroic mirror, NC nonlinear crystal, BS beam splitter, R reflector, SPD single-photon detector. Note: This figure is created by authors and does not contain any third-party materials or previously-created elements.

realized[36]. Furthermore, the concept of IFM was also applied to quantum imaging[37–39] and quantum communication[40–45].

The above-mentioned quantum imaging protocols can alleviate one or two specific requirements inherent in typical imaging. The goal of our work is to develop and experimentally demonstrate a quantum imaging protocol, in which all essential requirements of a typical imaging process (Fig. 1a) are simultaneously alleviated: (1) physical interaction — photons emitted from a light source impinge on the object and interact with it; (2) direct detection—scattered photons are detected to reveal the presence of object; (3) spatially resolved detector, such as a charge-coupled device (CCD)—spatial information is acquired. Here we report the realization of interaction-free, single-pixel quantum imaging with undetected photons (Fig. 1b) by combining IFM[6,7], SPI[9–13], and the IC[15–19] interferometer, as shown in Fig. 1c. Based on the principle of QIUP, the probe (idler) photon remains undetected throughout the imaging process. Information about the object of interest (in Fig. 1c, a cat) carried by the idler photon is transferred to the signal photon. However, unlike the previous QIUP realizations[5,23–25], IFM removes the requirement that the probe photon and the object interact. Finally, spatial information is obtained by SPI instead of using a CCD. SPI consists of the SLM and the single-pixel detector.

We have pushed the current quantum imaging ability to the extreme point where the detection requirements are minimized and both the illuminating photon and detected photon have no interaction with the object. Thus, our imaging protocol has the potential to characterize fragile or photon-sensitive systems, such as biological tissues[46] and quantum states of atomic ensembles[47,48]. Furthermore, spatially resolved single-photon detection is inefficient, costly and even unavailable in the challenging wavelength ranges, such as those in far-IR or even longer wavelength ranges. We can overcome the above limitations via minimum detection requirements. By employing economic, low-noise and high-efficiency visible single-photon detectors, we can realize long-wavelength interaction-free imaging.

## RESULTS

### The experimental scheme

The experimental setup is shown in Fig. 1d. It consists of three main parts, the IC interferometer, the IFM interferometer, and the SPI module. The IC interferometer is formed by double-passing a nonlinear crystal (NC) in a folded Michelson geometry[31]. As the pump passes the NC twice, it can generate a single pair of signal and idler photons via a forward (from left to right) or backward (from right to left after being reflected by the mirror $R_1$) spontaneous parametric down-conversion (SPDC) process. The forward and backward SPDC processes correspond to source-1 and source-2 in Fig. 1c, respectively. The pump laser with a wavelength of $\lambda_p = 532$ nm (green) collinearly generates from the NC a pair of frequency-nondegenerate correlated photons with wavelengths of $\lambda_s = 810$ nm (yellow) and $\lambda_i = 1550$ nm (red, the subscripts s and $_i$ denote the signal and idler photon). Both photon-pair sources are based on the type-I SPDC process, i.e., a horizontally polarized pump photon converts into vertically polarized signal and idler photons. We use a lithium niobate crystal (with thickness $L = 2$ mm and cutting angle $\theta = 68°$ for type-I phase matching) as the NC. Various dichroic mirrors (DM) are used to separate and combine frequency-nondegenerate photons. $DM_1$ transmits the pump and reflects both signal and idler photons. $DM_2$ transmits both pump and signal photons and reflects idler photons. $DM_3$ transmits signal photons and reflects idler photons. By adjusting the relative optical delays between the signal photon, the idler photon, and the pump with three motorized translation stages mounted on the mirrors $R_1$, $R_2$, and $R_3$, we establish path identity[18,19] of both forward and backward SPDC processes (see the Supplementary Note 1). Thereby, we obtain the quantum interferometer enabled by IC.

As shown in Fig. 1d, the idler photon generated from the forward SPDC process is reflected by $DM_2$ and injected into the

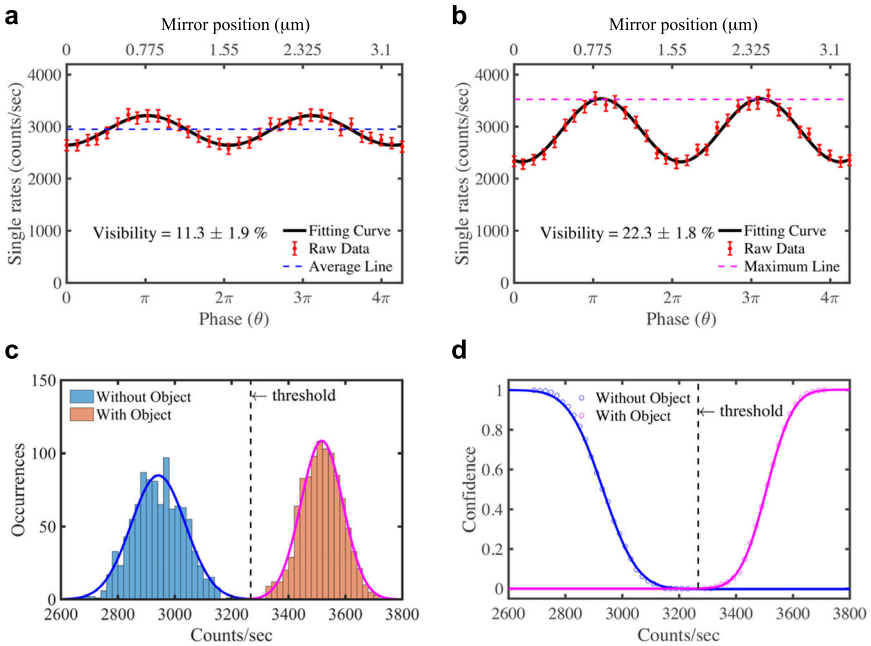


**Fig. 2 Interaction-free quantum sensing with undetected photons. a** By adjusting the phase $\theta$ of the signal photons, we obtain the residual interference of the signal photon in the absence of the object with a visibility of 11.3 ± 1.9%. **b** When the object is present, the idler photon performs a successful IFM and induces the interference of the signal photon. The experimental visibility is 22.3 ± 1.8%. The relative phase $\theta$ can be tuned by adjusting optical path difference of two arms in the nonlinear interferometer with motorized translation stages mounted on the mirrors $R_1$. **c** Counting histogram of the signal photon fitted by two Gaussian distributions. The width of each bin is 20 counts per second. The mean counts per second for sensing the presence (purple) and absence (blue) of the object are about 3,500 and 2,950, respectively. By setting a threshold (vertical black dash line), we clearly distinguish whether the object is present or not. **d** The confidence of the sensing is obtained by integrating the two Gaussian distributions shown in panel (**c**); a confidence level above 99.93% at the 3.4-sigma threshold is obtained. Error bars in panels (**a** and **b**) indicate two standard errors of the mean.

IFM module, realized by a Michelson interferometer. If the object is not in the IFM module, then this idler photon will deterministically exit from the Vac port, providing the relative phase $\phi$ of the IFM module to be 0. Consequently, no forward-generated idler photon goes back to the NC, and hence IC interference is prohibited. In this case, no IC interference of the signal and idler photons can be observed. On the other hand, if an opaque object is inserted into arm ③ of the IFM module, then the mere presence of this object will prohibit the interference of the IFM. With the probability of 25%, the idler photon generated in the forward SPDC will propagate back into the IC interferometer. Note that this 25% portion accounts for the idler photon passing the balanced beam splitter (BS) twice along arm ② of the IFM module. Thus, the path identity of the IC interferometer can be partially established, and hence signal photons show interference with 50% visibility. We can then infer the presence of the object by evaluating the interferogram of signal photons. We emphasize that the probe (idler) photon has never interacted with the object throughout the entire process. This is a subtlety of IFMs, at whose basis lies the wave-particle duality of a single photon. A single photon is indivisible because of its particle property and cannot split on a beam splitter[49]. Therefore, every idler photon that goes back to the IC interferometer must not have propagated through arm ③ of the IFM and hence would not have interacted with the object.

The single-pixel imaging with the signal photon is realized in the SPI module (see Fig. 1d). In SPI, one can reconstruct the multi-pixel image by interrogating the image with a set of spatially resolved masks and simultaneously recording the correlated intensity with a single-pixel detector. Mathematically, the image can be described by $\mathbf{I} = \mathbf{P} \cdot \mathbf{T}$, where $\mathbf{I}$ represents the pixelated image, $\mathbf{P}$ is a set of masks, and $\mathbf{T}$ is a collection of correlated photon counts (weighting) for the corresponding mask set. A commonly used set of spatially resolved masks is the Hadamard set[50,51]. We use a SLM to display the Hadamard mask to project the image onto a single-mode fibre-coupled single-photon detector (SPD). The single-pixel SPD records the signal-photon counts for each mask.

## Quantum sensing

As the first step of our experiment, we realized interaction-free quantum sensing with undetected photons by inserting an opaque object into the IFM module. In the absence of the object, the visibility of the IFM module was 93.9 ± 1.1% (100% for the ideal case). This imperfection of the IFM interference allowed the idler photon to go back to the IC interferometer with a low probability of about 2% at the destructive phase point $\phi = 0$. Imperfections of the IFM and other optical components in our experimental setup resulted in residual interference with small visibility for the signal photon, which was about 11.3 ± 1.9% (Fig. 2a). In the ideal case, this visibility of signal interference should be zero. Once the opaque object was inserted into arm ③ of the IFM module, a fraction of the idler photons generated by the forward SPDC were reflected back to the NC with no interaction with the object (see explanations above). These idler photons induced interference of signal photons with a visibility of 22.3 ± 1.8% (Fig. 2b). Therefore, the signal photon had different visibilities, depending on the presence of the object. Operationally, we use the fitted maximum counts ($\theta = \pi$) of the IC interference (purple dashed line in Fig. 2b) to denote a successful detection of the object with IFM and use the averaged counts (blue dashed line in Fig. 2a) to denote the absence of the object. The single counts of the signal photon thus allow us to decide whether or not the object is in the IFM module without interacting with it. See the Supplementary Note 1 for details of the interference visibilities.

In Fig. 2c, we show the counting histogram of the signal photon for interaction-free quantum sensing without detecting the probe

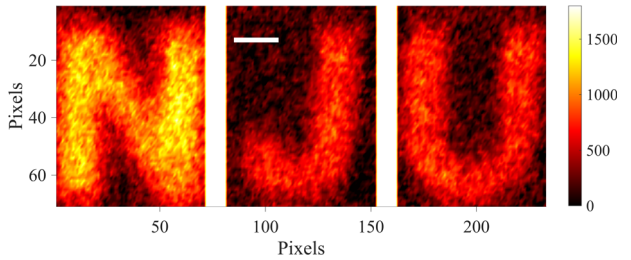


**Fig. 3 Interaction-free quantum imaging result of the 'NJU' characters with undetected photons.** In the presence of the plate in arm ③ of the interaction-free measurement module, two images are obtained with ICCD at phase setting ($\theta = \pi, \phi = 0$) and ($\theta = 0, \phi = \pi$) (see the Supplementary Fig. 4a and 4b). The difference between these two images is shown above. The signal photon inside the three characters has higher visibility than in outside regions. The three characters '**N**', '**J**' and '**U**' are measured independently. The length of the scale bar (white colour) in the figure is 200 μm.

photon (idler), fitted with two well-separated Gaussian functions. We clearly distinguish the presence (counts above threshold) and absence (counts below threshold) of the object with a confidence level above 99.93% at the 3.4-sigma threshold (indicated with the vertical black dash line in Fig. 2d).

## Quantum imaging

Next, we realized interaction-free imaging with undetected photons (IFIUP). We employed an intensified CCD camera (ICCD, Andor-iStar, DH334T-18U-73, shown in Fig. 1f) to image a spatially structured object, which is a 3D-printed 'NJU' logo (the abbreviation of Nanjing University). The region with the characters is transparent and the complementary region is opaque. Therefore, the character and the remaining regions correspond to the absence/presence of the object, respectively. These two regions have different interference visibilities. Using the method presented above, we can obtain different counts for these two regions and perform IFIUP, which is recorded with the ICCD. At the same phase setting as in previous quantum sensing ($\theta = \pi, \phi = 0$, see Fig. 1d), we obtained one image of the 'NJU' plate. Then, we adjusted the relative phase $\phi$ to π, and the signal phase $\theta$ to 0. At this phase setting, the idler photon deterministically propagates back into NC. The signal photon correlated with the idler photon propagating along the character region interferes constructively at this phase setting ($\theta = 0, \phi = \pi$). In Fig. 3, we show the subtraction of the obtained images for these two settings, highlighting the difference between constructive and destructive interference and enhancing the interference contrast. The size of each pixel in the image is 13 μm × 13 μm. For the details of imaging resolution, spatial properties of photon pairs and other discussions, please refer to the Supplementary Note 2–5.

Finally, using the SPI module shown in Fig. 1e, we realized the interaction-free, single-pixel quantum imaging with undetected photons. With the SPI method, the object can be reconstructed by multiplying each mask in the sampling set by the corresponding signal-photon counts, resulting in a set of weighted masks that can be summed up to form an image. Here, we employed a SLM device (ViALUX, V-650LNIR) to display the Hadamard masks[50,51], with a pixel number of 64 × 64 (the size of each pixel is 32.4 μm × 32.4 μm). We employed 1024 masks to perform SPI. For each mask, we recorded signal-photon counts at four settings, $C(\theta = \pi, \phi = 0)$, $C(\theta = 0, \phi = 0)$, $C(\theta = 0, \phi = \pi)$, and $C(\theta = \pi, \phi = \pi)$ and determined for each mask the signal-photon count $C_M$ (see the

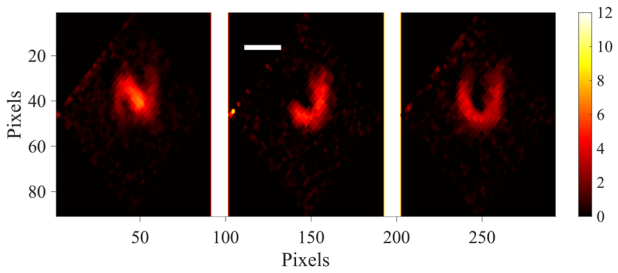


**Fig. 4 Interaction-free, single-pixel quantum imaging result of the 'NJU' plate with undetected photons.** The three characters '**N**', '**J**', and '**U**' are measured independently with the single-pixel imaging technique. Note that in our experiment, the micromirror of the SLM is rotated 45° at a mount. The edge of SLM can be vaguely seen at the upper left corner of the image. We rotate the reconstructed images by 45° to obtain the above images. The background noise in the signal-photon counts results in some speckles in the reconstructed images. Because of the structural difference of characters and limited detection area of the fiber-coupled detector, the visual result of character '**N**' is less prominent than '**J**' and '**U**'. The length of the scale bar (white colour) in the figure is 500 μm.

Supplementary Note 6):

$$C_M = C(\theta = 0, \phi = \pi) - C(\theta = \pi, \phi = \pi) - C(\theta = \pi, \phi = 0) + C(\theta = 0, \phi = 0) \quad (1)$$

Each mask is multiplied by the corresponding value of $C_M$ to give a set of weighted masks. By summing up all weighted masks, we reconstruct the images of the 'NJU' plate, shown in Fig. 4.

## DISCUSSION

We have demonstrated interaction-free, single-pixel quantum imaging with undetected photons, which is fundamentally different with typical imaging. By harnessing the wave-particle duality of single photons, interaction-free imaging is performed with the probe (idler) photons. Based on induced coherence, the image information carried by the idler photons, which have no interaction with the object, is transferred to the signal photons. Finally, using the SPI method, we reconstruct the image of the object solely with a sequence of signal-photon counts detected by a visible single-photon detector without spatial resolution. Therefore, our imaging protocol has alleviated all three requirements in the typical imaging scenario. We have pushed the capability of quantum imaging to the extreme point. Both the illuminating photon and probe photon have no physical interaction with the interested object. Furthermore, the detection requirement in quantum imaging is minimized to visible single-photon detectors without spatial resolution.

We note that the IFM efficiency can be further improved by using more advanced optical interferometric setups and low-loss optical switches[34–36]. In addition, broadband phase-matching conditions in nonlinear materials can be exploited to generate highly frequency-nondegenerate photon pairs, providing flexibility in the spectral range for both signal photon and idler photon. Thereby, our protocol can be extended into IR[23–25] or THz[26] single-pixel imaging without disturbing the sample using low-noise and high-efficiency visible single-photon detectors. We emphasize that the above statement of 'interaction-free' is only sensible for binary objects[37–39] due to the interference property of IFM. For grey or quantum objects, our experimental facility has the potential to realize single-pixel quantum interrogation[34] with undetected photons. Compared with conventional imaging, both interaction-free imaging and quantum interrogation based on single-photon interference can reduce sample exposure to intense light fields. Our measurement protocol may be beneficial for the probe of sensitive specimens, which is limited by unavailable photon-starved detection capabilities[23] and inevitable damage

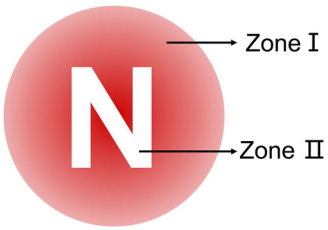


**Fig. 5 Illustration of the imaging plate.** It can be divided into opaque Zone I and transparent Zone II. Here we only use the character '**N**' to illustrate the imaging plate. Other characters follow the same rules.

induced by interaction[52–54]. As such, we hope this work will stimulate wide research interest in multiple fields, such as delicate material investigation[47,48] and life science[54].

## METHODS

For the '**NJU**' plate used in our imaging experiment, the character region is transparent (Zone II), and the complementary region (Zone I) is opaque, as shown in Fig. 5. If this plate is inserted into arm ③ of the IFM, the signal photons in the two regions will have different interference visibilities. The interference image of Zone I and Zone II can be described as

$$C_{\mathrm{I}}(\theta,\phi)=P_{\mathrm{I}(x,y)}\left[1-\frac{1}{2}\cos(\theta+\phi)\right], \tag{2}$$

$$C_{\mathrm{II}}(\theta,\phi)=P_{\mathrm{II}(x,y)}\left\{1+\frac{1}{2}[\cos\theta-\cos(\theta+\phi)]\right\}, \tag{3}$$

where $P_{\mathrm{I}(x,y)}$ and $P_{\mathrm{II}(x,y)}$ are zone-dependent photon-emission rates of the NC in Zone I and Zone II, respectively.

At the constructive interference point of the IFM, $\phi=\pi$, the entire interference image of the signal photon can be represented as

$$\begin{aligned}C(\theta,\phi=\pi)&=C_{\mathrm{I}}(\theta,\phi=\pi)+C_{\mathrm{II}}(\theta,\phi=\pi)\\&=P_{\mathrm{I}(x,y)}\left[1+\tfrac{1}{2}\cos\theta\right]+P_{\mathrm{II}(x,y)}[1+\cos\theta].\end{aligned} \tag{4}$$

By tuning the phase $\theta$, we can obtain the constructive and destructive images:

$$C_{\max}(\theta,\phi=\pi)=C(\theta=0,\phi=\pi)=\frac{3}{2}P_{\mathrm{I}(x,y)}+2P_{\mathrm{II}(x,y)}; \tag{5}$$

$$C_{\min}(\theta,\phi=\pi)=C(\theta=\pi,\phi=\pi)=\frac{1}{2}P_{\mathrm{I}(x,y)}. \tag{6}$$

At the destructive interference point of the IFM, $\phi=0$, the entire interference image of the signal photon can be expressed as

$$\begin{aligned}C(\theta,\phi=0)&=C_{\mathrm{I}}(\theta,\phi=0)+C_{\mathrm{II}}(\theta,\phi=0)\\&=P_{\mathrm{I}(x,y)}\left[1-\tfrac{1}{2}\cos\theta\right]+P_{\mathrm{II}(x,y)}.\end{aligned} \tag{7}$$

In this case, the constructive and destructive images are

$$C_{\max}(\theta,\phi=0)=C(\theta=\pi,\phi=0)=\frac{3}{2}P_{\mathrm{I}(x,y)}+P_{\mathrm{II}(x,y)}; \tag{8}$$

$$C_{\min}(\theta,\phi=0)=C(\theta=0,\phi=0)=\frac{1}{2}P_{\mathrm{I}(x,y)}+P_{\mathrm{II}(x,y)}. \tag{9}$$

To enhance the interference contrast of the imaging, we subtract Eq. (8) from Eq. (5) to obtain the final image:

$$C_{\max}(\theta,\phi=\pi)-C_{\min}(\theta,\phi=0)=P_{\mathrm{II}(x,y)}. \tag{10}$$

Then only the signal counts in the character region are left on the image. This data-processing method is employed in interaction-free quantum imaging with undetected photons by ICCD. In this method, we need to record the images of the signal photon at two settings, $(\theta=0,\phi=\pi)$ and $(\theta=\pi,\phi=0)$.

For the interaction-free, single-pixel quantum imaging with undetected photons, we employ the following method to process the imaging data:

$$\begin{aligned}&C_{\max}(\theta,\phi=\pi)-C_{\min}(\theta,\phi=\pi)-C_{\max}(\theta,\phi=0)\\&\quad+C_{\min}(\theta,\phi=0)=2P_{\mathrm{II}(x,y)}.\end{aligned} \tag{11}$$

In this case, we need to record signal-photon counts for each Hadamard mask at four settings, $(\theta=0,\phi=\pi)$, $(\theta=\pi,\phi=\pi)$, $(\theta=\pi,\phi=0)$ and $(\theta=0,\phi=0)$. This method can enhance the brightness of the image because the signal-photon counts obtained in Eq. (11) is twice as much as in Eq. (10). Processing the four recorded signal-photon counts based on Eq. (11), we get the corresponding counts of each Hadamard mask. Each mask in the sampling set is then multiplied by the corresponding counts to give a set of weighted masks. Then, we sum all weighted masks to reconstruct the final image[13].

## DATA AVAILABILITY

The data that support the findings of this study are available online at https://github.com/YiquanYang/Interaction-free-single-pixel-quantum-imaging-with-undetected-photons.

## CODE AVAILABILITY

The codes that support the findings of this study are available online at https://github.com/YiquanYang/Interaction-free-single-pixel-quantum-imaging-with-undetected-photons.

Received: 25 July 2022; Accepted: 26 December 2022;
Published online: 05 January 2023

## REFERENCES

1. Genovese, M. Real application of quantum imaging. *J. Opt.* **18**, 073002 (2016).
2. Moreau, P., Toninelli, E., Gregory, T. & Padgett, M. J. Imaging with quantum states of light. *Nat. Rev. Phys.* **1**, 367–380 (2019).
3. Pittman, T., Shih, Y. H., Strekalov, D. V. & Sergienko, A. V. Optical imaging by means of two-photon quantum entanglement. *Phys. Rev. A* **52**, R3429–R3432 (1995).
4. Strekalov, D. V., Sergienko, A. V., Klyshko, D. N. & Shih, Y. H. Observation of two-photon ghost interference and diffraction. *Phys. Rev. Lett.* **74**, 3600–3603 (1995).
5. Lemos, G. B. et al. Quantum imaging with undetected photons. *Nature* **512**, 409–412 (2014).
6. Dicke, R. H. Interaction-free quantum measurements: A paradox? *Am. J. Phys.* **49**, 925 (1981).
7. Elitzur, A. C. & Vaidman, L. Quantum mechanical interaction-free measurements. *Found. Phys.* **23**, 987–997 (1993).
8. Shapiro, J. H. & Boyd, R. W. The physics of ghost imaging. *Quantum Inf. Process* **11**, 949–993 (2012).
9. Shapiro, J. H. Computational ghost imaging. *Phys. Rev. A.* **78**, 061802 (2008). (R).
10. Duarte, M. F. et al. Single-pixel imaging via compressive sampling. *IEEE Signal Process. Mag.* **25**, 83–91 (2008).
11. Altmann, Y. et al. Quantum-inspired computational imaging. *Science* **361**, 660 (2018).
12. Edgar, M. P., Gibson, G. M. & Padgett, M. J. Principles and prospects for single-pixel imaging. *Nat. Photonics* **13**, 13–20 (2019).
13. Gibson, G. M., Johnson, S. D. & Padgett, M. J. Single-pixel imaging 12 years on: a review. *Opt. Exp.* **28**, 28190–28208 (2020).
14. Hadfield, R. H. Single-photon detectors for optical quantum information applications. *Nat. Photonics* **3**, 696–705 (2009).
15. Zou, X. Y., Wang, L. J. & Mandel, L. Induced coherence and indistinguishability in optical interference. *Phys. Rev. Lett.* **67**, 318–321 (1991).

16. Wang, L. J., Zou, X. Y. & Mandel, L. Induced coherence without induced emission. *Phys. Rev. A.* **44**, 4614–4622 (1991).
17. Herzog, T. J., Rarity, J. G., Weinfurter, H. & Zeilinger, A. Frustrated two-photon creation via Interference. *Phys. Rev. Lett.* **72**, 629–632 (1994).
18. Krenn, M., Hochrainer, A., Lahiri, M. & Zeilinger, A. Entanglement by path identity. *Phys. Rev. Lett.* **118**, 080401 (2017).
19. Hochrainer, A., Lahiri, M., Erhard, M., Krenn, M. & Zeilinger, A. Quantum indistinguishability by path identity and with undetected photons,. *Rev. Mod. Phys.* **94**, 025007 (2022).
20. Kalashnikov, D. A., Paterova, A. V., Kulik, S. P. & Krivitsky, L. A. Infrared spectroscopy with visible light. *Nat. Photonics* **10**, 98–101 (2016).
21. Vallés, A., Jiménez, G., Salazar-Serrano, L. J. & Torres, J. P. Optical sectioning in induced coherence tomography with frequency-entangled photons. *Phys. Rev. A.* **97**, 023824 (2018).
22. Paterova, A. V., Yang, H., An, C., Kalashnikov, D. A. & Krivitsky, L. A. Tunable optical coherence tomography in the infrared range using visible photons. *Quantum Sci. Technol.* **3**, 025008 (2018).
23. Kviatkovsky, I., Chrzanowski, H. M., Avery, E. G., Bartolomaeus, H. & Ramelow, S. Microscopy with undetected photons in the mid-infrared. *Sci. Adv.* **6**, eabd0264 (2020).
24. Paterova, A. V., Maniam, S. M., Yang, H., Grenci, G. & Krivitsky, L. A. Hyperspectral infrared microscopy with visible light. *Sci. Adv.* **6**, eabd0460 (2020).
25. Paterova, A. V., Yang, H., Toa, Z. S. D. & Krivitsky, L. A. Quantum imaging for the semiconductor industry. *Appl. Phys. Lett.* **117**, 054004 (2020).
26. Kutas, M. et al. Terahertz quantum sensing. *Sci. Adv.* **6**, eaaz8065 (2020).
27. Búzàs, A., Wolff, E. K., Benedict, M. G., Ormos, P. & Dér, A. Biological microscopy with undetected photons. *IEEE Access* **8**, 107539–107548 (2020).
28. Töpfer, S. et al. Quantum holography with undetected light. *Sci. Adv.* **8**, eabl4301 (2022).
29. Yurke, B., McCall, S. L. & Klauder, J. R. SU(2) and SU(1,1) interferometers. *Phys. Rev. A.* **33**, 4033–4054 (1986).
30. Hudelist, F. et al. Quantum metrology with parametric amplifier-based photon correlation interferometers. *Nat. Commun.* **5**, 3049 (2014).
31. Chekhova, M. V. & Ou, Z. Y. Nonlinear interferometers in quantum optics. *Adv. Opt. Photonics* **8**, 104–155 (2016).
32. Ou, Z. Y. & Li, X. Quantum SU(1,1) interferometers: basic principles and applications. *APL Photonics* **5**, 080902 (2020).
33. Du, W. et al. SU(2)-in-SU(1,1) Nested interferometer for high sensitivity, loss-tolerant quantum metrology. *Phys. Rev. Lett.* **128**, 033601 (2022).
34. Kwiat, P. G. et al.High-efficiency quantum interrogation measurements via the quantum Zeno effect. *Phys. Rev. Lett.* **83**, 4725–4728 (1999).
35. Kwiat, P., Weinfurter, H., Herzog, T., Zeilinger, A. & Kasevich, M. A. Interaction-free measurement. *Phys. Rev. Lett.* **74**, 4763–4766 (1995).
36. Ma, X. et al. On-chip interaction-free measurements via the quantum Zeno effect. *Phys. Rev. A.* **90**, 042109 (2014).
37. White, A. G., Mitchell, J. R., Nairz, O. & Kwiat, P. G. "Interaction-free" imaging. *Phys. Rev. A.* **58**, 605–613 (1998).
38. Zhang, Y. et al. Interaction-free ghost-imaging of structured objects. *Opt. Exp.* **27**, 2212–2224 (2019).
39. Hance, J. R. & Rarity, J. Counterfactual ghost imaging. *npj Quantum Inf.* **7**, 88 (2021).
40. Noh, T. Counterfactual quantum cryptography. *Phys. Rev. Lett.* **103**, 230501 (2009).
41. Liu, Y. et al. Experimental demonstration of counterfactual quantum communication. *Phys. Rev. Lett.* **109**, 030501 (2012).
42. Salih, H., Li, Z., Al-Amri, M. & Zubairy, M. S. Protocol for direct counterfactual quantum communication. *Phys. Rev. Lett.* **110**, 170502 (2013).
43. Cao, Y. et al. Direct counterfactual communication via quantum Zeno effect. *Proc. Natl Acad. Sci.* **114**, 4920–4924 (2017).
44. Alonso Calafell, I. et al. Trace-free counterfactual communication with a nano-photonic processor. *npj Quantum Inf.* **5**, 61 (2019).
45. Salih, H., McCutcheon, W., Hance, J. R. & Rarity, J. The laws of physics do not prohibit counterfactual communication. *npj Quantum Inf.* **8**, 60 (2022).
46. Stephens, D. J. & Allan, V. J. Light microscopy techniques for live cell imaging. *Science* **300**, 82–86 (2003).
47. Wolfgramm, F., Vitelli, C., Beduini, F. A., Godbout, N. & Mitchell, M. W. Entanglement-enhanced probing of a delicate material system. *Nat. Photonics* **7**, 28–32 (2012).
48. Eckert, K. et al. Quantum non-demolition detection of strongly correlated systems. *Nat. Phys.* **4**, 50–54 (2008).
49. Grangier, P., Roger, G. & Aspect, A. Experimental evidence for a photon anticorrelation effect on a beam splitter: a new light on single-photon interferences. *Europhys. Lett.* **1**, 173 (1986).
50. Pratt, W., Kane, J. & Andrews, H. C. Hadamard transform image coding. *Proc. IEEE* **57**, 58–68 (1969).
51. Sloane, N. J. A. & Harwit, M. Masks for Hadamard transform optics, and weighing designs. *Appl. Opt.* **15**, 107–114 (1976).
52. Putnam, W. P. & Yanik, M. F. Noninvasive electron microscopy with interaction-free quantum measurements. *Phys. Rev. A* **80**, 040902 (2009).
53. Turner, A. E., Johnson, C. W., Kruit, P. & McMorran, B. J. Interaction-free measurement with electrons. *Phys. Rev. Lett.* **127**, 110401 (2021).
54. Taylor, M. A. & Bowen, W. P. Quantum metrology and its application in biology. *Phys. Rep.* **615**, 1–59 (2016).

## ACKNOWLEDGEMENTS

We thank Anton Zeilinger for the inspiring discussion. This research was supported by the National Key Research and Development Program of China (Grants No. 2019YFA0308704, No. SQ2022YFE011462, and No. 2017YFA0303704), the National Natural Science Foundation of China (Grants No. 11690032 and No. 11321063), the NSFC-BRICS (Grant No. 61961146001), the Leading-Edge Technology Program of Jiangsu Natural Science Foundation (Grant No. BK20192001), the Fundamental Research Funds for the Central Universities, and the Innovation Program for Quantum Science and Technology (Grant No. 2021ZD0301500).

## AUTHOR CONTRIBUTIONS

Y.Y. and X.-s.M. designed the experiment. Y.Y., H. L., X. X., L.Z. and X.-s.M. performed the experiment. Y.Y. and X.-s.M. analysed the data and wrote the manuscript with input from all authors. S.Z. and X.-s.M. supervised the project.

## COMPETING INTERESTS

The authors declare no competing interests.

## ADDITIONAL INFORMATION

**Supplementary information** The online version contains supplementary material available at https://doi.org/10.1038/s41534-022-00673-6.

**Correspondence** and requests for materials should be addressed to Xiao-song Ma.

**Reprints and permission information** is available at http://www.nature.com/reprints

**Publisher's note** Springer Nature remains neutral with regard to jurisdictional claims in published maps and institutional affiliations.